Subunit exchange of multimeric protein complexes

REAL-TIME MONITORING OF SUBUNIT EXCHANGE BETWEEN SMALL HEAT SHOCK PROTEINS BY USING ELECTROSPRAY-MASS SPECTROMETRY

Frank Sobott[1], Justin L. P. Benesch[1*], Elizabeth Vierling[2], Carol V. Robinson[1]*

1. Department of Chemistry, Cambridge University,

Lensfield Road, Cambridge CB2 1EW, UK.

2. Department of Biochemistry & Molecular Biophysics, The University of Arizona,

Tucson AZ 85721-0106, USA.

*F. S. and J. L. P. B. contributed equally to this work.

Address correspondence to C. V. R.

E-mail: cvr24@cam.ac.uk, Tele: +44 1223 763846, Fax: +44 1223 763849.

Running Title

Subunit exchange of multimeric protein complexes

Summary

The subunit exchange of the small heat shock proteins (sHSPs) *Ps*HSP18.1 from pea and *Ta*HSP16.9 from wheat has been monitored in real-time using electrospray-mass spectrometry. By preserving the noncovalent interactions between subunits in the mass spectrometer, we show that these proteins are dodecameric. After mixing of *Ps*HSP18.1 and *Ta*HSP16.9 a distribution of hetero-dodecamers is formed. A comparison with spectra obtained from statistical modeling demonstrates that, after equilibration, the distribution of these hetero-complexes is governed by the starting ratio of the two components, rather than an inherent preference for certain stoichiometries. This suggests that the two different sHSP subunits interact in a very similar manner. Following the kinetics of this reaction by mass spectrometry reveals that exchange proceeds via sequential incorporation of subunits, with dimeric species being the principal units of exchange. Therefore we conclude that sHSP complexes are in rapid dissociation/re-association equilibria with sub-oligomeric forms. More generally these experiments illustrate a powerful approach for the real-time analysis of the evolution of transient species, and their relative populations, during the subunit exchange of multimeric protein complexes.

Introduction

The small heat shock protein (sHSP) family is both large and diverse, with members found in virtually all organisms. The sHSPs are induced under a variety of stresses and act to increase cellular tolerance to these conditions. Additionally they have been implicated in cancer, cataract, neurodegenerative diseases, and myopathy (1-4). It is not clearly understood how the sHSPs become involved in such diseases, but current models propose that they act primarily as molecular chaperones, preventing improper protein associations (5). This is evidenced by their ability to bind non-native proteins under different stress conditions, thereby preventing

their irreversible aggregation and consequent damage to the cell (6-11). These bound substrates can subsequently be refolded in an ATP-dependent manner upon interaction with the HSP70 system or DnaK (in eukaryotic and prokaryotic cells respectively) and co-chaperones (8-10,12,13).

The sHSPs are characterized by a conserved C-terminal 'α-crystallin' domain (14,15), and typically have subunit masses between 15 and 40kDa. The proteins assemble into large oligomers, containing 9 to >24 monomers, of varying heterogeneity. Some sHSPs, such as those from plants, form assemblies with well defined stoichiometries, whereas other sHSPs, including the mammalian proteins, form a range of oligomeric sizes (16). This polydispersity has limited the amount of structural information available, and consequently only two X-ray structures have thus far been reported for intact sHSPs: those of *Methanococcus jannaschii* HSP16.5 (17) and *Triticum aestivum* HSP16.9 (18). Compared to the wealth of such information available for other molecular chaperones, the sHSP family remains relatively poorly understood.

Figure 1 shows the structure of *Ta*HSP16.9 along the crystallographic three-fold axis (figure 1A), and along one of the two-fold axes (figure 1B). *Ta*HSP16.9 is composed of twelve subunits arranged into two hexameric rings. Six of the monomers in the dodecamer are fully resolved, but the others have disordered N-terminal arms which remain unresolved in the crystal structure. In *Mj*HSP16.5, which forms a spherical 24-mer (17), the N-terminal arms were revealed by cryo-electron microscopy to partially fill the central cavity (16). Each *Ta*HSP16.9 subunit interacts with four others, forming five different interfaces. The strongest of these dimeric interactions are thought to be those arising from ß-strand donation between two partner monomers in the same ring (figure 1A). These dimeric 'building blocks', which take the same form in *Mj*HSP16.5, interact with those adjacent through hinged C-terminal extensions; and there is additional stabilization of the dodecamer by the pairwise intertwining

of N-terminal helices (figure 1B) (18). Despite having what appears to be a tightly bound and rigid structure, *Ta*HSP16.9 has been shown to undergo a structural change and form sub-oligomeric species at higher temperatures. Furthermore, in the same study, *Ta*HSP16.9 has been shown to interact with its close homologue *Pisum sativum* HSP18.1 (also a cytosolic class I sHSP) to form complexes which show intermediate migration behavior in non-denaturing gel electrophoresis. Though the identity of these new complexes remains unclear, they were proposed to be hetero-dodecamers formed by subunit exchange between the two sHSPs (18).

Such subunit exchange had previously been shown to occur between sHSPs from other plants (19), and the bacterium *Bradyrhizobium japonicum* (20). In both cases, however, exchange was shown only to occur if the proteins were of the same class. In mammals, various sHSPs are capable of exchanging subunits. In the vertebrate eye lens, α-crystallin forms hetero-aggregates containing αA- and αB-subunits at an approximate 3:1 ratio (15), and these have been shown to have a dynamic quaternary structure (21-24). In addition, αA can undergo exchange with HSP27 (25), and mixed aggregates of αB, HSP27 and HSP20, as well as HSPB2 and HSPB3 have been found in muscle cells (26). It is not clear what the function of such facile intermolecular subunit exchange in sHSPs may be, but with several sHSPs being expressed in the same cellular compartments (14,27-29) it seems likely that the formation of such hetero-complexes will also occur *in vivo*.

Mass spectrometry (MS) is well established as a method for measuring the masses of individual proteins. When coupled with nano-electrospray ionization (nanoESI), MS is being increasingly recognized as a technique capable of measuring the mass and probing the properties of intact macromolecular assemblies (30,31). Using a protocol of appropriate solution conditions, and maintaining many low energy collisions to absorb the excess

translational energy of the ions during their desolvation, large macromolecular assemblies can be transported intact through the mass spectrometer. Molecules with masses of over 2MDa have been mass-measured in this way (32). We, and others, have previously used mass spectrometry to characterize and investigate the properties of different molecular chaperones including GroEL (33), HSP90 (34), SecB (35,36), and MtGimC/Prefoldin (37). In the case of MtGimC, the subunit stoichiometry and interactions were elucidated by MS by following the assembly of the complex in real-time. While fluorescence resonance energy transfer (FRET) has been used to monitor the subunit exchange between sHSP oligomers (23,25), it is unable to identify individual species and their abundances, and consequently only presents an averaged picture of the reaction. MS on the other hand has not been widely applied to the investigation of such problems, yet with the ability to preserve subunit interactions, the rapid data acquisition possible, and mass accuracy attainable, it is a potentially powerful method.

Here we present the application of nanoESI MS to the investigation of the subunit exchange reaction between two sHSPs: *Ta*HSP16.9 and *Ps*HSP18.1. We find that we can measure the relative populations of hetero-complexes differing by only one protein subunit, and can thereby monitor the exchange reaction at the molecular level in real-time.

Experimental Procedures

Materials. *Ta*HSP16.9 from *Triticum aestivum* (wheat) was expressed in *E. coli* and purified as described previously (18). Its amino acid sequence is given by GenBank accession number S21600 with one change T7S and absence of the N-terminal Met (sequence mass 16722.0Da). *Ps*HSP18.1 from *Pisum sativum* (pea) was expressed in E. coli and purified as described previously (38). The sequence is given by GenBank accession number P19243 with one change P37L and absence of the N-terminal Met (17970.3Da). Cesium iodide and ammonium

acetate were obtained from Sigma. Buffer solutions were prepared from purified water (Millipore, Watford, UK).

Nano-electrospray mass spectrometry. Mass spectra were recorded on a tandem-mass spectrometer (Q-Tof, Micromass, Manchester/UK) modified for high-mass operation (39). Nano-ESI capillaries were prepared in-house from borosilicate glass tubes of 1mm OD and 0.5mm ID (Harvard Apparatus, Holliston, MA/USA) using a Flaming/Brown P-97 micropipette puller (Sutter Instruments, Hercules, CA/USA), and gold-coated using an SEM sputter-coater (Polaron, Newhaven, UK). The capillary tips were cut under a stereo-microscope to give inner diameters of 1-5µm, and typically 0.5-2µl of solution were loaded for sampling. The conditions within the mass spectrometer (specifically pressures and accelerating potentials) were adjusted to preserve noncovalent interactions. The following experimental parameters were typically used (positive ion mode): capillary voltage 1.7kV, cone gas 100L/h, sample cone 180V, extractor cone 20V, collision energy 4V, ion transfer stage pressure 4.0×10^{-3} mbar, quadrupole analyzer pressure 1.8×10^{-5} mbar, Tof analyzer pressure 4.7×10^{-7} mbar, and spectrum acquisition frequency 3.9kHz.

External calibration of the spectra was achieved using solutions of cesium iodide. Data were acquired and processed with MassLynx software (Micromass, Manchester/UK). All spectra are shown with minimal smoothing and without background subtraction. The series of peaks which arise for each species are due to different numbers of protons attached to the molecular ion. Their mass-to-charge (m/z) ratios follow the equation $m/z = (M_{protein} + z\, M_{H+})/z$, where $M_{protein}$ is the protein mass, M_{H+} the mass of a proton, and z the number of protons (charges). Multiple protonation is induced by the electrospray process and occurs up to a maximum approximately corresponding to the number of basic, accessible sites in the protein (40). Transformation of the signal from an m/z to mass scale is performed using MassLynx, by multiplication of the m/z value of each peak with the number of charges z, and subtraction of

z times the proton mass. We used tandem-MS, where ions are selected by the quadrupole mass analyzer of the Q-Tof and subjected to collision-induced dissociation (CID) in a gas-filled collision cell, to reveal the composition of the noncovalent complexes (39).

Sample preparation and handling. sHSP samples were stored at -20°C, and buffer-exchanged twice into 200mM aqueous ammonium acetate (pH 7) using micro-centrifuge columns (Bio-Spin, Bio-Rad Laboratories, Hercules, CA/USA). Buffer exchange and sample introduction were conducted at room temperature (24±2°C). For the subunit exchange equilibration experiments, different volumes of the two protein solutions were combined to give the appropriate molar ratios, vortexed briefly, and allowed to equilibrate at room temperature for approximately 2h before analysis. Incubating the samples for longer periods of time did not result in further reaction, only a deterioration in the mass spectra. To monitor the exchange kinetics in real-time, we combined *Ps*HSP18.1 and *Ta*HSP16.9 at a ratio of 3:1 to give a final volume of 20µL, at a total protein concentration of 37.5µM (dodecamer). A 2µL aliquot of this sample was loaded into a capillary and introduced immediately into the mass spectrometer. We were able to acquire the first data within 40s of mixing, and acquired data continuously for approximately 40min. The remaining sample was kept at room temperature, and analyzed after about 9h to verify the endpoint of the reaction. To confirm that continuous spraying of the solution, while the reaction proceeded, did not effect the exchange reaction, individual aliquots were analyzed at different time intervals, and the resulting spectra were found to be indistinguishable from those obtained during the continuous sampling experiment (data not shown).

Kinetic data. To extract kinetic information from the time-resolved data, we combined spectra over eight-second intervals around 29 time points, in addition to the end-point. Due to the overlap of a number of peaks in the mass spectrum which arises from the heterogeneity of the mixed oligomers, only the intensities (peak heights) of those signals which could be assigned

unambiguously were taken into account. The following peaks were monitored: m/z 5906, 5737 for $(16.9)_{12}$; 6746, 6541 for $(18.1)_{12}$; 6312, 6130 for $(18.1)_{11}(16.9)_1$; 6669, 6466, 6095 for $(18.1)_{10}(16.9)_2$; 6630, 6430, 6239, 6059 for $(18.1)_9(16.9)_3$; and 6590, 6390, 6202, 6024 for $(18.1)_8(16.9)_4$. The intensities of each component were expressed as percentages of the total intensity, and the scale adjusted to the initial and final abundances in solution (given by a theoretical binomial distribution, see below). Initial decay rates were calculated by plotting the natural logarithm of the intensity versus time, and fitting linear lines of best fit.

Simulation of mass spectra. The simulated spectrum was constructed using SigmaPlot 2001 (SPSS Science, Chicago, IL/USA). Theoretical intensities of the 13 different dodecamers were calculated based on a binomial distribution of the components *Ps*HSP18.1 and *Ta*HSP16.9 at a ratio of 3:1, assuming an equal preference for each composition. The statistical propensity, P_n,of individual dodecamers containing n times the 18.1 subunit is given by

$$P_n = \frac{12!}{n!(12-n)!} (P_{18.1})^n (P_{16.9})^{12-n}, \qquad \text{(eq.1)}$$

where $P_{18.1}$ and $P_{16.9}$ are the relative abundances of HSP18.1 and 16.9 subunits in solution (0.75 and 0.25 respectively for a 3:1 ratio). The last two terms describe the probability for finding certain numbers of each subunit in the complex, while the first term accounts for the number of possible arrangements of these subunits within the complex. A three-parameter Gaussian curve was fitted across the tops of the peaks in the spectra of the two individual sHSPs. The midpoint and width of these curves were used to create similar ones for the theoretical charge state distributions of the hetero-dodecamers. Their maxima were scaled to the theoretical intensity of the various species. Three-parameter Lorentzian curves were used to model individual peaks, with the peak width at half height of 10Da (as measured from the charge states in the mass spectra of the homo-dodecamers). The intensity was given by

solution of the Gaussian function for that charge state. Combining all simulated peaks resulted in the total simulation.

Results

Characterization of sHSP complexes. Figure 2 shows nanoESI mass spectra of the small heat shock proteins *Ps*HSP18.1 and *Ta*HSP16.9 under conditions optimized for the transmission of intact noncovalent complexes. The dominant feature of both spectra is the group of peaks around an m/z value of 6000 (left panels), with very little additional signal outside this range. The right hand panels of figure 2 show a transformation of the peaks in this range from an m/z to a mass scale. For *Ta*HSP16.9 (figure 2A) only one major species **a** is detected, with a molecular mass of 200790Da. This mass compares well with the mass calculated for twelve *Ta*HSP16.9 monomers (200663.6Da). Therefore we conclude that *Ta*HSP16.9 forms a dodecamer in solution, as expected from its X-ray structure (figure 1) (18). The observation that the experimental mass is slightly higher than that calculated from the sequence, in this case by about 126Da, is common for mass spectra of noncovalent complexes, and is most likely due to the binding of solvent molecules and buffer ions, presumably at the subunit interfaces (41).

The mass spectrum recorded for a solution of *Ps*HSP18.1 is similar to that of *Ta*HSP16.9, although the peaks appear at slightly higher m/z and carry on average more charges (figure 2B). Here we observe three distinct complexes of similar mass: 215850Da (**b**), 215215Da (**c**) and 214452Da (**d**). Again the complexes consist of twelve subunits, as seen by comparison with a theoretical mass for the dodecamer of 215643.7Da. More than one third of the total HSP18.1 signal resides in peaks **c** and **d**. Isolation of these species in the quadrupole analyzer of the instrument and subsequent collision-induced dissociation (CID) reveals that dodecamer **b** consists of twelve identical copies of the full-length protein, whereas **c** and **d** each contain one subunit with a truncation of the first six (**c**) and 13 (**d**) N-terminal amino acids,

respectively (CID spectra not shown). These truncations are likely to have arisen during protein expression and purification. As their presence does not destabilize the complex relative to CID (spectra not shown) they do not appear to compromise the formation of the dodecamer in these quantities.

Products of subunit exchange. We used mass spectrometry to determine the products of the reaction between *Ps*HSP18.1 and *Ta*HSP16.9 at four different molar ratios (6:1, 3:1, 1:3, and 1:6). Spectra recorded after equilibration of mixtures at molar ratios of 6:1 and 1:6 of the two sHSPs are shown in figure 3A and B respectively. Many peaks are observed which are not present in the spectra of the individual sHSPs. Mass measurement shows that they arise from dodecamers containing subunits of both sHSPs. At a 6:1 ratio (figure 3A) peaks are observed which correspond to a range of hetero-dodecamers containing between eight and twelve *Ps*HSP18.1 monomers, and the most intense signals are due to the species $(18.1)_{10}(16.9)_2$. The minor peaks not labeled in this spectrum arise from hetero-dodecamers containing truncated *Ps*HSP18.1 subunits. For the opposite 1:6 ratio, dodecamers can be seen which contain between eight and twelve *Ta*HSP16.9 monomers (figure 3B). Here the species with the highest intensity is $(18.1)_2(16.9)_{10}$. The charge state ensemble has been shifted to lower m/z values relative to the 6:1 ratio, due to the presence of fewer *Ps*HSP18.1 monomers within the dodecamers. The comparatively low *Ps*HSP18.1 concentration also explains the apparent absence of peaks due to dodecamers containing truncated subunits. Similarly, at 18.1:16.9 ratios of 3:1 (upper part of figure 4A) and 1:3 (data not shown) we find the most intense species to be $(18.1)_9(16.9)_3$ and $(18.1)_3(16.9)_9$, respectively.

For the mixtures studied above, it appears that the intensities of hetero-dodecamers formed by subunit exchange is governed by the relative concentration of the individual sHSPs in solution. In other words, the distribution of hetero-dodecamers appears to be centered on the ratio of the two components in the mixture. For example, the most abundant hetero-

dodecamer formed from an HSP18.1:16.9 ratio of 3:1 is $(18.1)_9(16.9)_3$. To establish whether the distribution of the different hetero-complexes is determined solely by the abundance of the sHSP subunits in solution, we simulated a 'statistical' spectrum, assuming no preference for the uptake of monomers of either sHSP, nor any inherent preference for particular stoichiometries. The histogram in figure 4 (inset) shows the theoretical binomial distribution of hetero-complexes for an HSP18.1:16.9 ratio of 3:1, according to equation 1. From this distribution it can be seen that the dominant species is indeed $(18.1)_9(16.9)_3$, amongst a broad range of different compositions ranging from $(18.1)_4(16.9)_8$ (n=4) to the homo-dodecamer $(18.1)_{12}$ (n=12). Using the theoretical abundances of the different species from the histogram, and their theoretical charge state distribution (see experimental procedures), we plotted simulated ESI spectra for all dodecamers (lower part of figure 4). The sum of all these overlapping species corresponds well to the actual mass spectrum recorded for a 3:1 ratio (upper part of figure 4). The major difference between the simulated and experimental data is the appearance of a higher background signal, which we attribute primarily to overlapping peaks arising from multiple charge states of both full length and truncated *Ps*HSP18.1 subunits with coincident m/z values, which were not taken into account in the simulation. The fact that the distribution of species matches that predicted by the simulation supports the picture of a statistical incorporation of different subunits into the dodecamer.

Kinetics of subunit exchange. We followed the kinetics of the subunit exchange between HSP18.1 and 16.9 by monitoring the reaction continuously over a period of 40 minutes to elucidate details of the reaction mechanism. Figure 5 shows three time-points recorded for a solution of 18.1:16.9 at a ratio of 3:1. In this experiment spectra have been averaged over 4min. intervals to improve signal-to-noise ratios. The t=0 spectrum represents a superposition of HSP18.1 and 16.9 spectra (cf. figure 2A and B), with their relative intensities adjusted according to their molar ratio. The first indication of subunit exchange is apparent after 2min.

when the signal of the hetero-complex $(18.1)_{10}(16.9)_2$ is clearly observed (spectra not shown), and after 8-12min. this species dominates the spectrum. Eventually, after 36-40min., we observe the equilibrium distribution of hetero-complexes, as described in the previous section. The intensities of the peaks assigned to $(18.1)_{12}$ and $(16.9)_{12}$ were plotted as a function of time in figure 6. The abundance of these homo-dodecamers follows an exponential decay function over approximately the first 10min., consistent with a first-order reaction. By plotting the natural logarithm of this decay at the beginning of the reaction (inset figure 6), we can extract the rate constants for dissociation from the slope of the linear line of best fit. They are $0.24\pm0.05 min^{-1}$ and $0.20\pm0.04 min^{-1}$ at 24°C for HSP18.1 and 16.9 respectively. After 10 minutes very little of the homo-dodecamers remains, and a variety of hetero-complexes has been formed. The relative abundances of the four predominant hetero-species are plotted in figure 7. From the data it can be seen that hetero-complexes containing an even number of each type of subunits are formed more rapidly than those containing an odd number, i.e. $(18.1)_{10}(16.9)_2$ is produced faster than $(18.1)_{11}(16.9)_1$, and $(18.1)_8(16.9)_4$ faster than $(18.1)_9(16.9)_3$. All curves except that for $(18.1)_9(16.9)_3$ go through a maximum before they reach their equilibrium levels. While a simple look at the abundance of each species at equilibrium (see previous chapter) suggests a purely statistical exchange of subunits, the evolution of specific hetero-complexes reveals a different picture: that of even-numbered species being kinetically favored.

Discussion

We have investigated the composition and oligomeric status of two plant small heat shock proteins and followed their subunit exchange reaction in real-time by mass spectrometry. *Ta*HSP16.9 and *Ps*HSP18.1 have been maintained intact in the gas phase as dodecamers, which is their native form in solution (18,38). Truncation of up to 13 N-terminal amino acids

in one *Ps*HSP18.1 monomer does not appear to affect dodecamer formation, which is similar to the closely related polydisperse αA-crystallins where it has also been shown that truncation of up to 19 amino acids from the N-terminus does not significantly change the subunit organization of the complex (25).

While sHSP complexes appear to be rather rigid, stable entities, their structure is in fact very dynamic, enabling them to interact and form hetero-complexes by mutual exchange of subunits. With nanoESI MS, we investigated equilibrated mixtures of HSP18.1 and 16.9 at different initial ratios, and found a distribution of hetero-complexes of varying composition dependent on the initial subunit ratio. In spite of the symmetrical, well-ordered arrangement of subunits in the dodecamer, we see no indication for preferred stoichiometries. Instead the sHSP subunits seem to be indistinguishable in the dodecamer, as the end products of the exchange reaction are purely statistical.

Subunit exchange can in principle be thought to proceed via two alternative mechanisms: dissociation into smaller subcomplexes followed by re-association into dodecamers, or by a 'collision'/'encounter complex' mechanism. The latter can be ruled out because it would show second-order kinetics. In the dissociation-association model on the other hand, the experimentally determined first-order kinetics indicate that dissociation of dodecamers is rate-determining. Subunits constantly dissociate from the dodecamer and re-associate. This steady-state equilibrium is shifted towards the dodecamers, with the low level of subcomplexes limiting the rate of the overall exchange reaction. Consequently we observe significantly higher proportions of intact complex than dissociation products in the mass spectra (figure 2).

For the related αA-crystallin it was also found that dissociation of the intact protein complexes is rate-limiting, suggesting that the oligomers exist in a similar equilibrium with sub-oligomeric species (25). A first-order rate constant for subunit exchange between

fluorescence-labeled αA-crystallin and unlabeled αA- or αB-crystallin of $3.8x10^{-2}min^{-1}$ was reported. By comparison, we determined the rate constants for the decay of HSP18.1 and 16.9 as $0.20min^{-1}$ and $0.24min^{-1}$ respectively, which is approximately six times faster than for αA-crystallin and about two orders of magnitude faster than for wild-type transthyretin (42). Since the decay rate constants of both HSP18.1 and 16.9 are comparable, the free enthalpies of activation for the dissociation of the dodecamers into smaller subunits must also be of similar magnitude. We believe therefore that the subunit interfaces of the two sHSPs, as well as their interactions in the complex, are closely similar.

About 3-4min. after the exchange reaction was initiated, only 50% of the homo-complexes remain (figure 6), while several new hetero-complexes have already formed, figure 7. The shape of the curves, which go through a maximum, is typical of a sequential reaction, since subsequent exchange reactions only become important after enough intermediate species have built up. The observed kinetic preference for even-numbered hetero-complexes indicates that dimeric sHSP subunits are the predominant exchange units. This is in accordance with insight gained from the X-ray structure of HSP16.9 (figure 1), where close interactions between neighboring monomers have been found, suggesting that dimers are the 'building blocks' of the dodecameric protein complex (18). While dimer exchange is faster and thus clearly favored, the dimeric interaction must however at some stage be compromised, since hetero-complexes with an uneven number of subunits of each kind are also formed. This slower pathway could either involve exchange via monomers, or proceed via hetero-dimers which were formed in an exchange reaction between the homo-dimers in solution. After equilibration, the subunit composition of the dodecamers becomes statistical, no longer indicating a preference for exchange of dimers. However, kinetic monitoring of the reaction has revealed dimers as the predominant units of exchange.

Thus the picture of a very dynamic, yet surprisingly stable sHSP complex emerges, with dimeric subunits moving in and out of the oligomer on a rapid timescale. This fast association equilibrium is independent of the presence of other sHSPs, but it becomes apparent in the mutual exchange of subunits. The dynamic nature of the complexes could be essential for their role as molecular chaperones, enabling them to associate with non-native client proteins and shield them from aggregation, as has been suggested for other sHSPs (11). It could also provide a model for the *de novo* assembly of the dodecamers from the monomers in the cell. In cases where several different sHSPs are expressed in the same cellular compartment, we can expect them to readily exchange subunits with other members of the same class, and thus form complexes with a mixed composition. Although not much is known about the biological relevance of such sHSP hetero-complexes, it has been found that α-crystallin in the human eye lens, which is composed of a 3:1 ratio of αA- to αB-crystallin, has greater thermal stability than either protein alone, and is therefore more efficient in protecting cells from damage and stress (22). It is also conceivable that the substrate specificity and activity could be moderated by an exchange of subunits with related small heat shock proteins.

We have shown that using mass spectrometry we can investigate the subunit exchange reaction of these two closely related sHSPs, revealing the precise subunit composition of species throughout the entire exchange reaction. The ability of mass spectrometry to distinguish between protein assemblies differing in only one subunit, and simultaneously measure their relative abundance, makes it a convenient and effective method for the study of such complexes. Moreover, real-time analysis of the reaction reveals the build up of transient populations, hence allowing us to draw conclusions about the reaction mechanism. Using such an approach, the dynamics of a diverse range of multimeric protein complexes can be investigated.

Acknowledgements

We thank Eman Basha and Kenneth Friedrich (University of Arizona) for protein expression and purification, Rob van Montfort for useful discussions and help with figure 1, Mark Tito for initial MS experiments, Christine Slingsby and Orval Bateman (Birkbeck College, London) for helpful discussions, and the whole C.V.R. mass spectrometry group at Cambridge University for their support. J.L.P.B. receives support from EPSRC, E.V. from the National Institutes of Health (GM-42762) and the U.S. Department of Agriculture (NRICGP), and C.V.R. from the Royal Society.

References

1. Arrigo, A.-P., and Muller, W. E. G. (2002) *Small Stress Proteins*. Progress in Molecular and Subcellular Biology. (Arrigo, A.-P., and Muller, W. E. G., ed.), Springer
2. van Montfort, R., Slingsby, C., and Vierling, E. (2002) in *Protein Folding in the Cell* Vol. 59, pp. 105-156
3. Gaestel, M., Vierling, E., and Buchner, J. (1997) in *Guidebook to Molecular Chaperones and Protein Folding Catalysts* (Gething, M., ed), pp. 269-272, Oxford University Press
4. van den Ijssel, P., Norman, D. G., and Quinlan, R. A. (1999) *Curr. Biol.* 9, R103-R105
5. Haslbeck, M., and Buchner, J. (2002) in *Small Stress Proteins* (Arrigo, A.-P., and Muller, W. E. G., ed), pp. 37-59, Springer
6. Lindner, R. A., Carver, J. A., Ehrnsperger, M., Buchner, J., Esposito, G., Behlke, J., Lutsch, G., Kotlyarov, A., and Gaestel, M. (2000) *Eur. J. Biochem.* 267, 1923-1932
7. Kim, R., Kim, K. K., Yokota, H., and Kim, S. H. (1998) *Proc. Natl. Acad. Sci. U. S. A.* 95, 9129-9133
8. Ehrnsperger, M., Graber, S., Gaestel, M., and Buchner, J. (1997) *Embo J.* 16, 221-229
9. Lee, G. J., Roseman, A. M., Saibil, H. R., and Vierling, E. (1997) *Embo J.* 16, 659-671

10. Török, Z., Goloubinoff, P., Horvath, I., Tsvetkova, N. M., Glatz, A., Balogh, G., Varvasovszki, V., Los, D. A., Vierling, E., Crowe, J. H., and Vigh, L. (2001) *Proc. Natl. Acad. Sci. U. S. A.* 98, 3098-3103
11. Haslbeck, M., Walke, S., Stromer, T., Ehrnsperger, M., White, H. E., Chen, S. X., Saibil, H. R., and Buchner, J. (1999) *Embo J.* 18, 6744-6751
12. Lee, G. J., and Vierling, E. (2000) *Plant Physiol.* 122, 189-197
13. Veinger, L., Diamant, S., Buchner, J., and Goloubinoff, P. (1998) *J. Biol. Chem.* 273, 11032-11037
14. Kappé, G., Luenissen, J. A. M., and de Jong, W. W. (2002) in *Small Stress Proteins* (Arrigo, A.-P., and Muller, W. E. G., ed), pp. 1-17, Springer
15. de Jong, W. W., Caspers, G. J., and Leunissen, J. A. M. (1998) *Int. J. Biol. Macromol.* 22, 151-162
16. Haley, D. A., Bova, M. P., Huang, Q. L., McHaourab, H. S., and Stewart, P. L. (2000) *J. Mol. Biol.* 298, 261-272
17. Kim, K. K., Kim, R., and Kim, S. H. (1998) *Nature* 394, 595-599
18. van Montfort, R. L. M., Basha, E., Friedrich, K. L., Slingsby, C., and Vierling, E. (2001) *Nat. Struct. Biol.* 8, 1025-1030
19. Helm, K. W., Lee, G. J., and Vierling, E. (1997) *Plant Physiol.* 114, 1477-1485
20. Studer, S., and Narberhaus, F. (2000) *J. Biol. Chem.* 275, 37212-37218
21. Datta, S. A., and Rao, C. M. (2000) *J. Biol. Chem.* 275, 41004-41010
22. Sun, T. X., and Liang, J. J. N. (1998) *J. Biol. Chem.* 273, 286-290
23. Bova, M. P., Ding, L. L., Horwitz, J., and Fung, B. K. K. (1997) *J. Biol. Chem.* 272, 29511-29517
24. van den Oetelaar, P. J. M., van Someren, P., Thomson, J. A., Siezen, R. J., and Hoenders, H. J. (1990) *Biochemistry* 29, 3488-3493
25. Bova, M. P., Mchaourab, H. S., Han, Y., and Fung, B. K. K. (2000) *J. Biol. Chem.* 275, 1035-1042
26. Sugiyama, Y., Suzuki, A., Kishikawa, M., Akutsu, R., Hirose, T., Waye, M. M. Y., Tsui, S. K. W., Yoshida, S., and Ohno, S. (2000) *J. Biol. Chem.* 275, 1095-1104
27. Waters, E. R., Lee, G. J., and Vierling, E. (1996) *J. Exp. Bot.* 47, 325-338
28. Waters, E. R., and Vierling, E. (1999) *Mol. Biol. Evol.* 16, 127-139
29. Waters, E. R. (1995) *Genetics* 141, 785-795

30. Loo, J. A. (2000) *Int. J. Mass Spectrom.* 200, 175-186

31. Hernández, H., and Robinson, C. V. (2001) *J. Biol. Chem.* 276, 46685-46688

32. Tito, M. A., Tars, K., Valegard, K., Hajdu, J., and Robinson, C. V. (2000) *J. Am. Chem. Soc.* 122, 3550-3551

33. Rostom, A. A., and Robinson, C. V. (1999) *J. Am. Chem. Soc.* 121, 4718-4719

34. Garnier, C., Lafitte, D., Jorgensen, T. J. D., Jensen, O. N., Briand, C., and Peyrot, V. (2001) *Eur. J. Biochem.* 268, 2402-2407

35. Bruce, J. E., Smith, V. F., Liu, C. L., Randall, L. L., and Smith, R. D. (1998) *Protein Sci.* 7, 1180-1185

36. Smith, V. F., Schwartz, B. L., Randall, L. L., and Smith, R. D. (1996) *Protein Sci.* 5, 488-494

37. Fändrich, M., Tito, M. A., Leroux, M. R., Rostom, A. A., Hartl, F. U., Dobson, C. M., and Robinson, C. V. (2000) *Proc. Natl. Acad. Sci. U. S. A.* 97, 14151-14155

38. Lee, G. J., Pokala, N., and Vierling, E. (1995) *J. Biol. Chem.* 270, 10432-10438

39. Sobott, F., Hernández, H., McCammon, M. G., Tito, M. A., and Robinson, C. V. (2002) *Anal. Chem.* 74, 1402-1407

40. Kebarle, P. (2000) *J. Mass Spectrom.* 35, 804-817

41. Nettleton, E. J., Sunde, M., Lai, Z., Kelly, J. W., Dobson, C. M., and Robinson, C. V. (1998) *J. Mol. Biol.* 281, 553-564

42. Schneider, F., Hammarström, P., and Kelly, J. W. (2001) *Protein Sci.* 10, 1606-1613

Figure Legends

Figure 1: X-ray structure of the *Ta*HSP16.9 dodecamer (**A**: top view, bottom disk in grey for clarity; **B**: side view). The strongest dimer interactions are between subunits of the same color (but different shading) and are formed by ß-strand donation. Images were generated using SwissPDB and POV-Ray (PDB accession codes 1GME and R1GMESF).

Figure 2: NanoESI mass spectra of the small plant heat shock proteins *Ta*HSP16.9 (**A**) and *Ps*HSP18.1 (**B**) under conditions where noncovalent interactions are preserved in the mass spectrometer. Left panel: mass-to-charge (m/z) scale; right panel: transformed to mass scale.

The peaks represent multiply protonated dodecameric complexes. For the molecular masses of species **a**-**d** see text.

Figure 3: Products of subunit exchange between *Ps*HSP18.1 and *Ta*HSP16.9 at molar ratios of 6:1 (**A**) and 1:6 (**B**) after equilibration of the mixture. The major species are labeled for each charge state; the numbers in the colored circles indicate the number of *Ps*HSP18.1 subunits in the hetero-dodecamers.

Figure 4: Simulated and measured electrospray-mass spectra of the products of subunit exchange between *Ps*HSP18.1 and *Ta*HSP16.9 at a molar ratio of 3:1. Theoretical intensities of the individual species were calculated based on a binomial distribution of the components, as expected for freely interchangeable subunits (see inset; cf. eq. 1). The summation over all species (lower black trace) is in close agreement with the experimental spectrum (upper black trace).

Figure 5: Subunit exchange between *Ps*HSP18.1 and *Ta*HSP16.9 at a molar ratio of 3:1 monitored in real-time by mass spectrometry. The labels are the same as for figure 3. For t=0 (**A**) spectra of HSP18.1 and 16.9 have been superimposed using MassLynx, with the intensities adjusted for their molar ratio.

Figure 6: Decay of homo-dodecamers of *Ps*HSP18.1 and *Ta*HSP16.9 as monitored by mass spectrometry (cf. figure 5; summation of. relative intensities over selected charge states). The fitted lines are for illustrative purposes only. The inset shows a logarithmic plot of the first few data points, which is used to determine rate constants of the reaction.

Figure 7: Relative concentrations of the most abundant hetero-dodecamers as a function of time during subunit exchange between *Ps*HSP18.1 and *Ta*HSP16.9 at a molar ratio of 3:1 (cf. figure 5). The fitted lines are for illustrative purposes only.

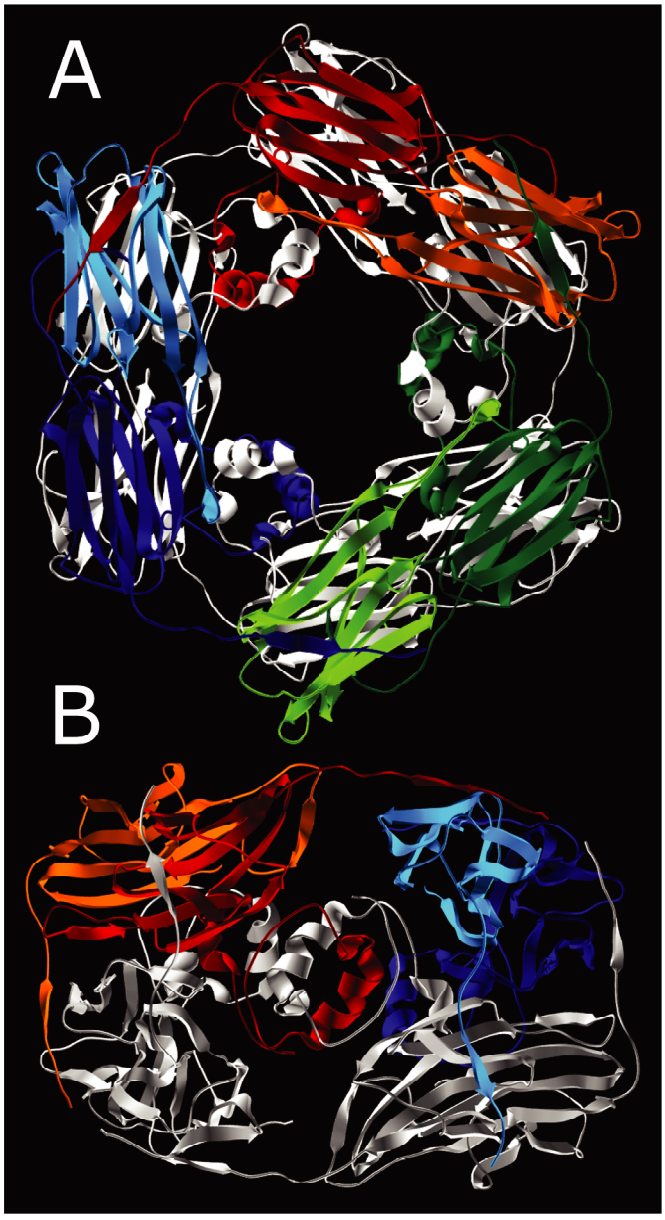

Figure 1

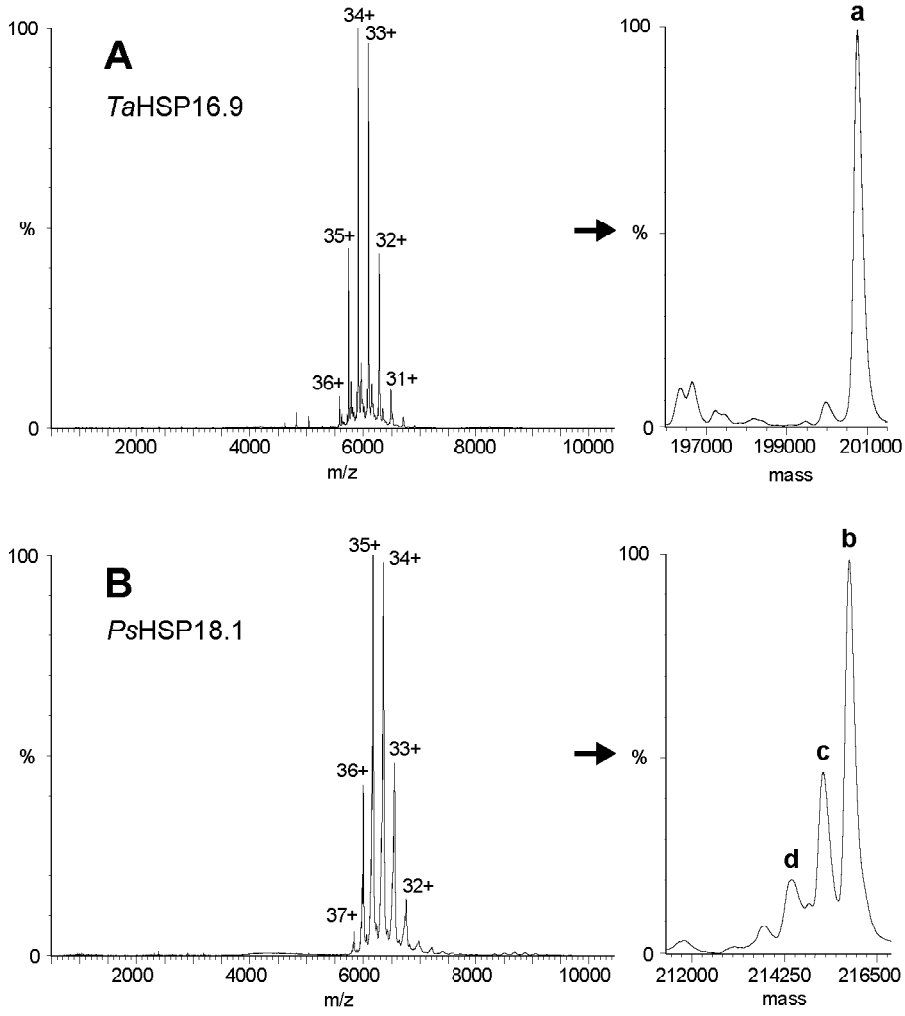
A
TaHSP16.9
34+
33+
35+
32+
36+
31+
100
%
0
2000
4000
6000
8000
10000
m/z
a
197000
199000
201000
mass
B
PsHSP18.1
35+
34+
33+
36+
32+
37+
b
c
d
212000
214250
216500

Figure 2

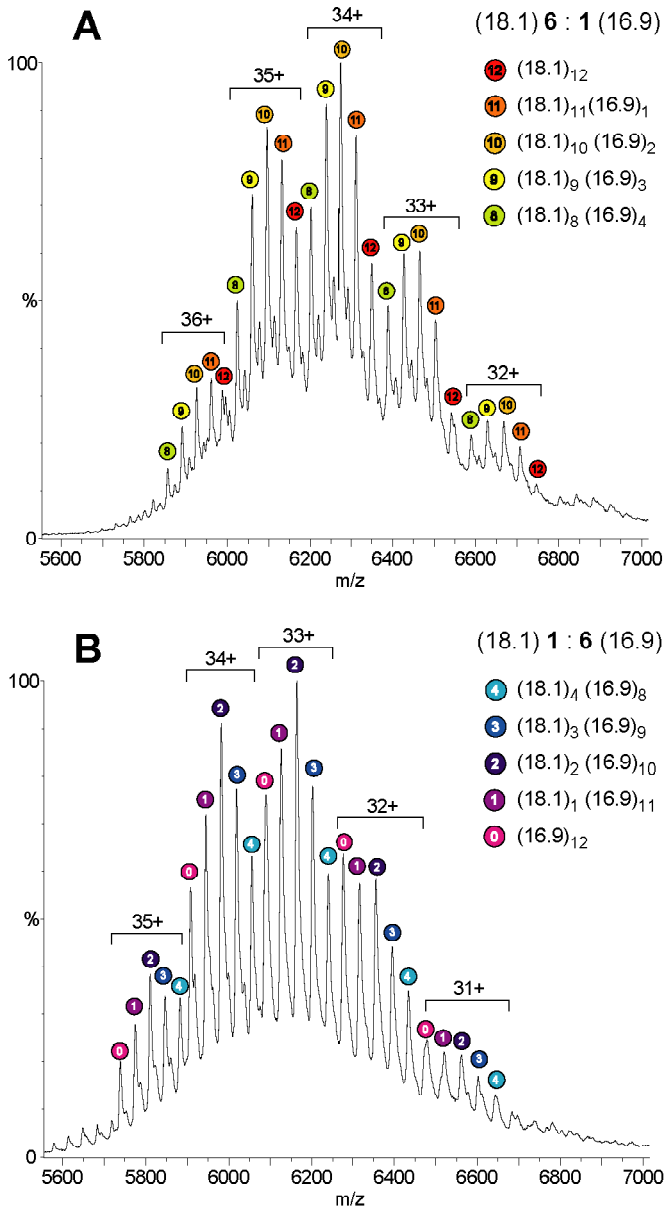
A
(18.1) 6 : 1 (16.9)
(18.1)12
(18.1)11(16.9)1
(18.1)10 (16.9)2
(18.1)9 (16.9)3
(18.1)8 (16.9)4
34+
35+
33+
36+
32+
100
%
0
5600
5800
6000
6200
6400
6600
6800
7000
m/z
B
(18.1) 1 : 6 (16.9)
(18.1)4 (16.9)8
(18.1)3 (16.9)9
(18.1)2 (16.9)10
(18.1)1 (16.9)11
(16.9)12
33+
34+
32+
35+
31+
100
%
0
5600
5800
6000
6200
6400
6600
6800
7000
m/z

Figure3

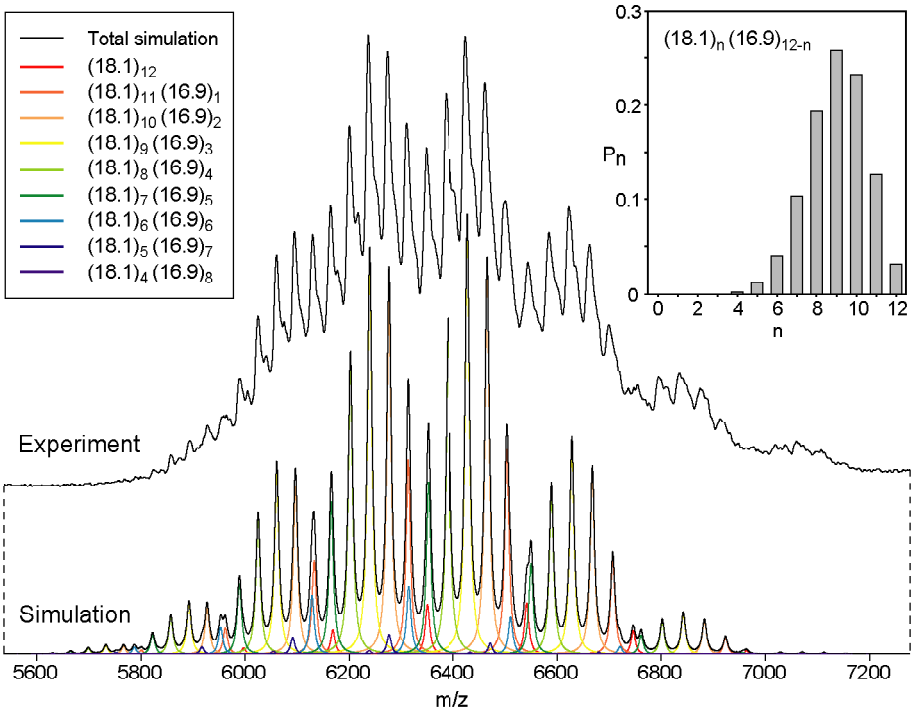
Total simulation
(18.1)12
(18.1)11 (16.9)1
(18.1)10 (16.9)2
(18.1)9 (16.9)3
(18.1)8 (16.9)4
(18.1)7 (16.9)5
(18.1)6 (16.9)6
(18.1)5 (16.9)7
(18.1)4 (16.9)8
(18.1)n (16.9)12-n
Pn
n
Experiment
Simulation
m/z

Figure4

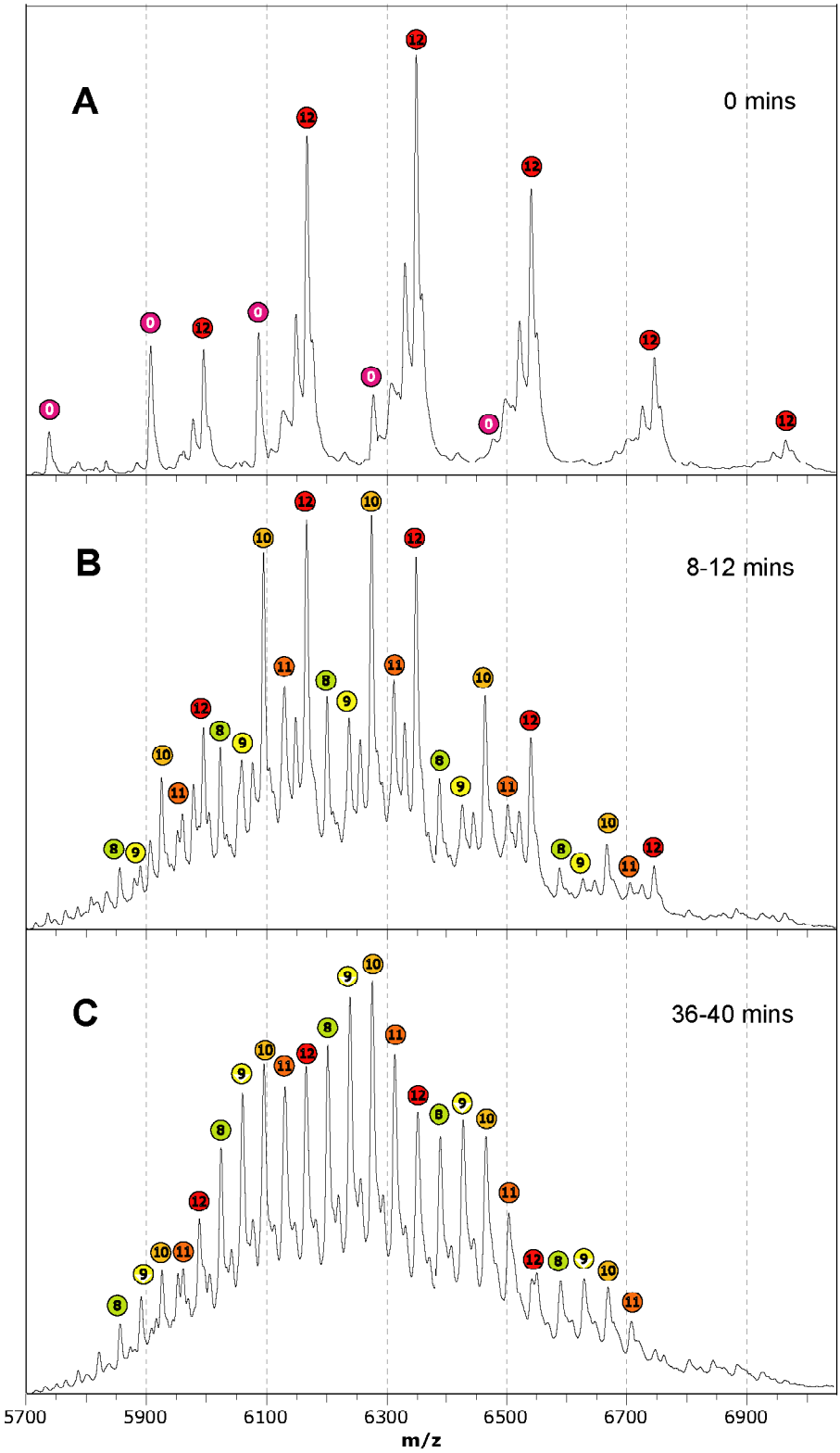
A
0 mins
B
8-12 mins
C
36-40 mins
5700
5900
6100
6300
6500
6700
6900
m/z

Figure 5

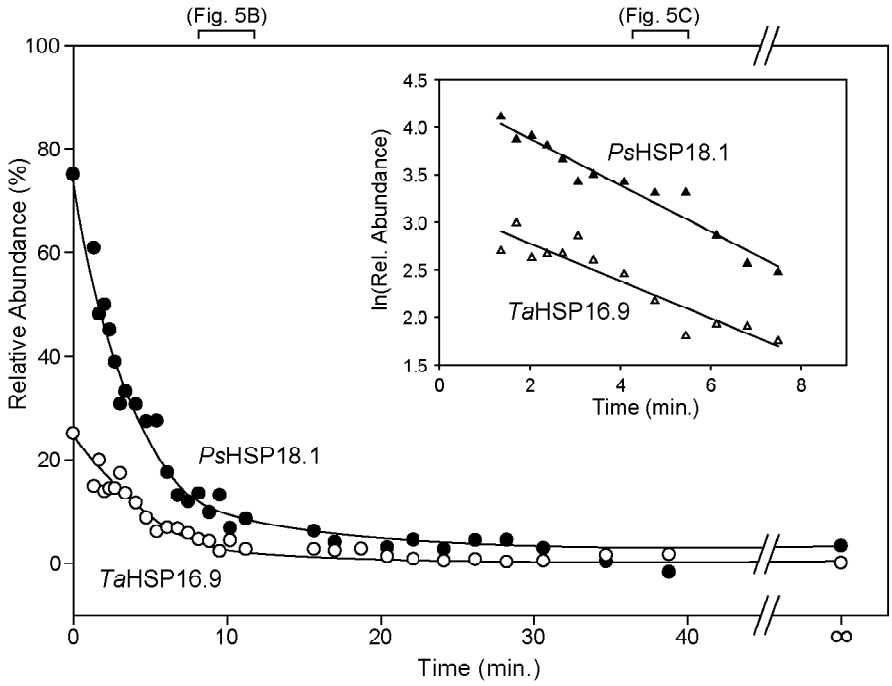
(Fig. 5B)
(Fig. 5C)
Relative Abundance (%)
Time (min.)
PsHSP18.1
TaHSP16.9
ln(Rel. Abundance)
Time (min.)
PsHSP18.1
TaHSP16.9

Figure6

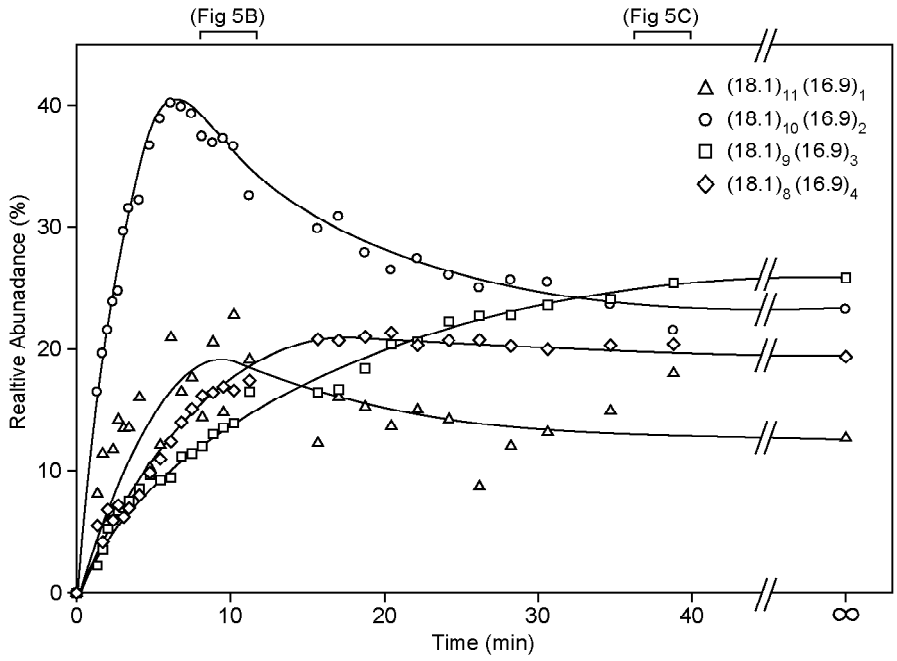
(Fig 5B)
(Fig 5C)
$(18.1)_{11}(16.9)_1$
$(18.1)_{10}(16.9)_2$
$(18.1)_9(16.9)_3$
$(18.1)_8(16.9)_4$
Realtive Abunadance (%)
0
10
20
30
40
Time (min)
0
10
20
30
40
∞

Figure7